Kovove Mater. 61 2023 91–101
DOI: 10.31577/km.2023.2.91

The effect of laser pre-oxidation of stainless steel on joining to polyamide by the LAMP method

Reza Ghanavati[1], Eslam Ranjbarnodeh[1]*, Reza Shoja-Razavi[2], Gholamreza Pircheraghi[3]

[1]*Department of Materials and Metallurgical Engineering, Amirkabir University of Technology, Tehran, Iran*
[2]*Faculty of Materials and Manufacturing Engineering, Malek-Ashtar University of Technology, Tehran, Iran*
[3]*Department of Materials Science and Engineering, Sharif University of Technology, Tehran, Iran*

Received 21 September 2022, received in revised form 15 November 2022, accepted 6 February 2023

Abstract

Among the factors affecting the efficiency of laser-assisted metal and polymer (LAMP) joints, the surface condition of the joint components is one of the most important ones. So, the present study explored the effect of laser pre-oxidation of stainless steel 304 (SS304), as a novel pretreatment method, on SS304/polyamide 6 joint strength. The assessments revealed that in spite of the potential of surface pre-oxidation of SS304 for improving joint strength, the strength of the joint was reduced by ~ 25 % in practice because, firstly, the wettability of the metal by the polymer was reduced due to the reduction of heat transfer by the metal in the pre-oxidized zone and secondly, the oxide layer formed on SS304 surface had a weak adherence due to the kinetic presence of Fe_2O_3. Hence, when using pre-oxidation, it is necessary to consider the nature of the oxide layer on the metal surface and the optimal variables of the joining process for the new conditions to achieve appropriate strength.

K e y w o r d s: LAMP method, stainless steel 304, polyamide 6, oxidation, wettability, adherence

1. Introduction

Using transportation instruments, like automobiles and planes, increases the emission of pollutants, including CO_2, due to fossil fuel consumption, so it has become a global challenge. A solution proposed is curbing fuel consumption by reducing the weight of structures [1], which can be achieved by employing light metals like magnesium, aluminum, and titanium and polymer-based materials like carbon fiber reinforced thermoplastics (CFRTP) in the automotive and aerospace industries [2]. Metal-polymer hybrid joints contribute to reducing the weight of components and structures and consequently reduce energy use in these industries. They will also lend manufacturers more flexibility in designing [3]. Nonetheless, the proper joining of dissimilar materials, especially metal-to-polymer joining, is still a big challenge in developing hybrid components and structures. Conventional metal-to-polymer joining methods, including adhesive bonding and mechanical joining, have their advantages, but they suffer from numerous limitations, such as limited joining speed, the induction of stress concentration zones, and zones susceptible to crack initiation and propagation [3]. To tackle these limitations, some methods have been developed for metal-to-polymer joining, which has come to be generally called thermal joining. They include ultrasonic joining [4, 5], friction spot joining [6, 7], friction stir joining [8], friction lap joining [9], laser joining [10–13], and resistance joining [14].

Laser-assisted metal and polymer direct joining (LAMP joining in short) is a subset of laser joining methods that has interested many researchers for various reasons, such as high joining speed, prevention of excessive polymer degradation at the joint, and flexibility in designing and manufacturing. As demonstrated by Katamaya et al. [10, 15], joining metal to polymer incorporates the mechanisms of chemical bonding between the polymer surface and oxide film over the metal surface, physical bonding due to the Van der Waals forces, and mechanical bonding due to

*Corresponding author: e-mail address: islam_ranjbar@aut.ac.ir

the locking of polymer parts into the surface roughness of the metal. These mechanisms were also verified by different techniques in the laser joining of stainless steel to different polymer pairs [16, 17]. As such, researchers have conducted extensive studies to explore the effect of joining process variables on joint quality and strength, including surface conditions of the joint components. For instance, in a study on joining cyclic olefin polymer and stainless steel 304, Arai et al. [18] explored the effect of polymer surface pre-oxidation by the UV radiation method in the ozone atmosphere on joint strength. Jung et al. [19] investigated the effect of surface pre-oxidation of the metal component by furnace heating within the air atmosphere on the joint strength between electro-galvanized iron (EGI) and acrylonitrile butadiene styrene (ABS). They reported that a ZnO layer at an optimal thickness could reinforce joint strength. Zhang et al. [20] studied the effect of pre-anodizing on shear strength in a joint between aluminum alloy A6061 and carbon fiber-reinforced polyamide 6. They observed that anodizing pre-treatment improved the shear strength of the joint reinforcing mechanical interlocks at the joint interface and the chemical bond between the joint components in the form of Al-O-PA6. Rodríguez-Vidal et al. [21] assessed the effect of modifying metal surface morphology by laser-assisted application of regular surface grooves on the strength of a joint between DP1000 dual-phase steel and glass fiber reinforced polyamide 6. Also, Sheng et al. [22] studied surface modification of stainless steel by two methods of abrasive paper scratching and laser texture processing to strengthen the joint to CFRTP and showed that laser texture processing would lead to higher shear strength. To improve the joint strength between aluminum alloy 7075 and CFRTP, Jiao et al. [23] proposed a hybrid surface modification method in which polyamide was incorporated into the joint interface, and the aluminum alloy surface was machined. The results revealed that the method performed well in enhancing joint strength by reinforcing mechanical interlocks at the joint interface. For the Al/CFRTP butt joint, Ye et al. [24] showed that among the pre-treatments of laser micro-texturing, anodizing, and hybrid of both, the former with optimal parameters (laser scanning distance and times) would result in maximum bond strength of 20 MPa.

The previous works have mainly focused on the effect of surface conditions of joint components on the strength irrespective of environmental issues, such as anodizing or laser texturing, which will result in toxic and hazardous by-products in the former and material waste in the latter. On the other hand, stainless steel 304 (SS304), which is widely used in hybrid structures, has been less addressed in research, so less focus has been put on the effect of its surface conditions on the strength of metal-polymer joints. Therefore, this research aimed to study laser pre-oxidation of SS304, as a novel pretreatment method, for joining to polyamide 6 (PA6) and to investigate its effect on joint strength using a tensile-shear test, hardness test, roughness measurement, differential scanning calorimetry, and imagery and elemental analysis at the cross-section and fracture surfaces of the joints.

Table 1. The chemical composition of stainless steel 304 (wt.%)

Fe	C	Cr	Mn	Ni	P	S	Si
Base	0.05	18.4	1.6	8.2	0.04	0.008	0.6

Table 2. Technical specifications of the Nd: YAG laser joining device used

Specification	Description
Laser type	Nd: YAG solid-state (continuous/pulse)
Laser wavelength	1064 nm
Average power	700 W
Frequency	1–1000 Hz
Lamp	Xenon
Pulse width	0.25–25 ms
Pulse energy	0.5–75 J
Peak power	10 kW
Spot diameter in focus mode	1 mm
Input power	20 kW
Power supply	Three-phase 300 V

2. Materials and methods

2.1. Base materials and joining process

Joint components were prepared with a size of 30 mm × 80 mm from a PA6 sheet with a thickness of 2 mm and an SS304 sheet with a thickness of 0.8 mm whose chemical composition is presented in Table 1. The back of the SS304, where it was supposed to come into contact with the PA6, was rubbed with a sandpaper P100 to increase the surface energy in the joint zone. Then, all surfaces were cleaned and degreased with acetone before joining.

For the first joint type, the SS304 and PA6 sheets were placed on one another in a lap joint design with a 40 mm overlap (half of a sheet's length) so that the stainless steel sheet was at the top and the PA6 sheet was at the bottom (due to the opacity of the polymer against the laser beam). Then, they were manually fixed stiffly with fixtures (Fig. 1a). An IQL-20 Nd: YAG solid-state laser (Table 2) was used to perform the joining process with a laser power of 200 W

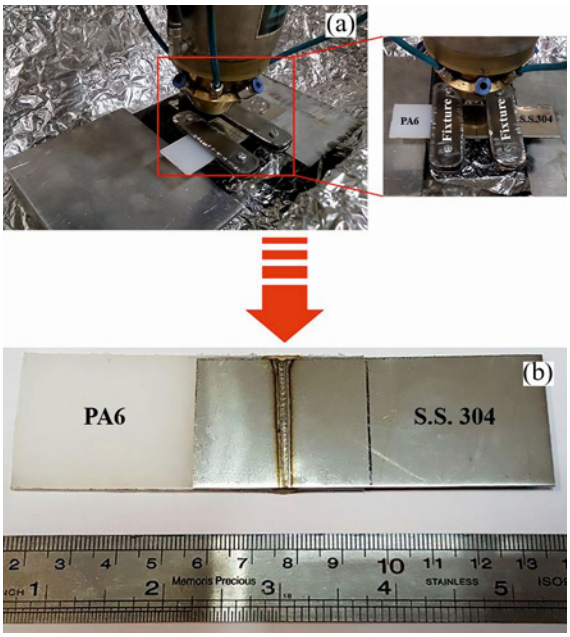

Fig. 1. (a) The fixed lap joint under the laser head and (b) the joint between stainless steel 304 and polyamide 6 (without surface pre-oxidation).

and a scanning velocity of 7 mm s^{-1} (approximately equivalent to laser input energy of 28 J mm^{-1}) under an argon gas shield with a flow rate of 15 L min^{-1} as continuous, single-pass and traverse in the middle of the join components' overlap zone. The joining process parameters, especially laser input energy level, were selected based on our previous work [25] to make the joint with minimum defects caused by the thermal degradation of the polymer and the maximum joint strength. Figure 1b shows the joint between stainless steel 304 and polyamide 6.

For the second joint type, to determine the effect of the metal surface pre-oxidation, the SS304 was surface-oxidized by laser beam scanning in the air atmosphere with a power of 200 W and a scanning velocity of 10 mm s^{-1}. Laser scanning for the surface oxidation was performed in the middle of the joint components' overlap zone on the back surface of the SS304, where it would be in contact with the polymer, and the joining would be done in that zone. Then, the pre-oxidized surface of the SS304 was placed in contact with the PA6 sheet, and the joining process was performed similarly to the joining process of the first joint type.

2.2. Tests and evaluation

2.2.1. Roughness measurement, macrostructural examination, and elemental analysis

After the surface oxidation pre-treatment on the SS304, the surface roughness in the oxidized and non-oxidized zones was measured with a profilometer for comparison, and the oxidized surface was examined with a field emission scanning electron microscope (FE-SEM) equipped with energy dispersive X-ray spectroscopy (EDS) (a MIRA2 LMU model, TESCAN Inc.) for morphological assessment and semi-quantitative elemental analysis. After the joining process, cross-sections were taken from the middle of the join line of both joint types (without and with surface pre-oxidation) by a water jet. The cross-sections were polished with a water-based solution at a very low force, time, and round. The interface in both joints was then subjected to imagery and elemental analysis with the scanning electron microscope. Also, after the tensile-shear test of the joint specimens, which is explained in detail in the next section, the polymer and metal-side fracture surfaces were subjected to imagery and elemental analysis by the same microscope. To inhibit the accumulation of electrical charge and to improve the image quality, the polymer specimens were coated with a thin film of gold by the sputtering technique.

2.2.2. Assessment of mechanical properties

The tensile-shear test was performed with a tensile machine (a Sun 2500 model, GALDABINI Inc.) at a maximum 2.5 t load to find out the strength of the joints. Since the joints were of the lap type, two sheets with the same thickness of the joint components were used as the alignment tab at the top and bottom of the joints in the tensile grips. Also, the crosshead rate of the tensile machine was set at 0.5 mm min^{-1} in the tensile-shear test. Further, the angular distortion (α, in degree) of the joints was estimated just like Ref. [26] by Eq. (1) as follows to consider its effect on the mechanical behavior of the joints:

$$\alpha = \arctan\left(\frac{h}{x}\right), \tag{1}$$

where h is the vertical displacement of the joint edge (mm) and x is the distance between the joint seam and joint edge (= 60 mm).

The hardness of the polymer component of the joints was measured with a Shore D hardness measurement device (SNATAM Inc.). The hardness of the polymer was measured (according to the ASTM D2240 standard) in two zones, including base polymer and polymer fracture surface at the joint zone, to investigate the impact of temperature variations during the joining process and, consequently, polymer microstructure variations on their hardness and strength. It should be noted that at least three tests were performed for each mechanical assessment, and the mean values were reported.

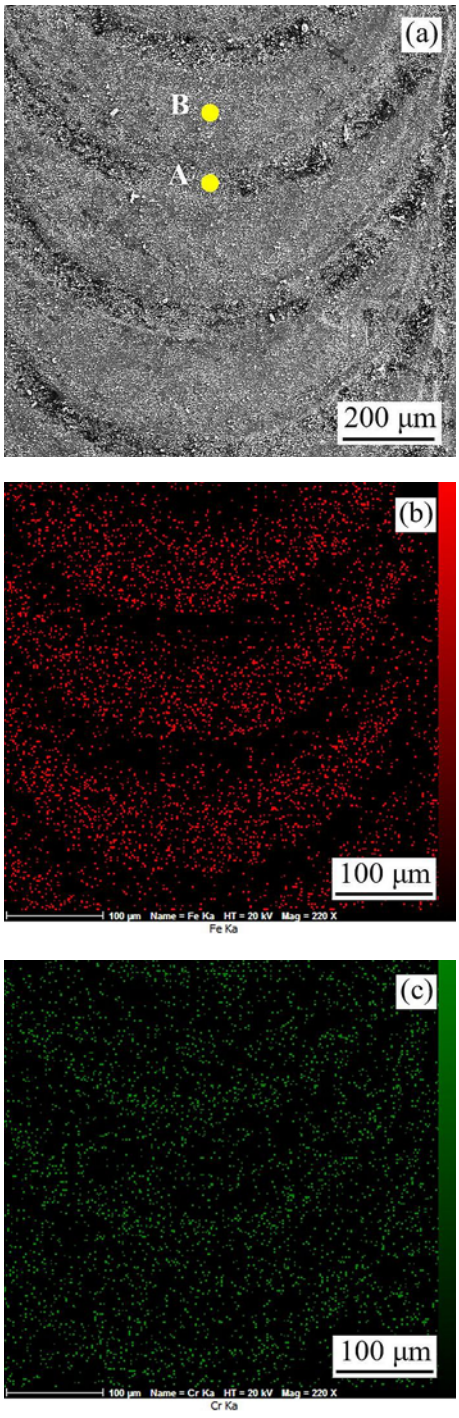

Fig. 2. (a) The morphology and elemental distribution maps of (b) Fe and (c) Cr on the oxidized surface of the SS304.

2.2.3. *Differential scanning calorimetry*

Differential scanning calorimetry (DSC) was used to determine the polymer crystallinity change in the joint zone due to the joining process. In this test, a part of the base polymer was considered the control sample, and the temperature variation range was set at 25–250 °C with a heating rate of 10 °C min^{-1}. Then, 4–12 mg of the polymer was sampled from the joint zone of each joint specimen and placed in the device tank filled with a nitrogen atmosphere for analysis. Given that the melting heat of PA6 at 100 % crystallinity is 230 J g^{-1} and after calculating the dipped region of each curve by the software, the crystallinity percentage of each sample was determined by Eq. (2) as follows [27]:

$$\%\text{Crystallinity} = \frac{|\Delta H_\text{m} - \Delta H_\text{c}|}{\Delta H_\text{m}^\circ}, \qquad (2)$$

in which ΔH_m, ΔH_c, and ΔH_m° (J g^{-1}) are the heat of melting, the heat released during solidification, and the heat of polymer melting in a 100 % crystallinity state, respectively. The difference between ΔH_m, ΔH_c is the area of the dipped region of each DSC curve.

Table 3. The results of elemental point analysis at points A and B in Fig. 2a

Analysis point	Element	Mean atomic percent	Relative count
Point A	O	31.5	384
	Cr	57.32	547.47
	Fe	11.18	132.4
Point B	O	30.14	627.43
	Cr	4.62	314.12
	Fe	65.24	1348.29

3. Results and discussion

Figure 2 displays the morphology and results of the elemental analysis of the oxidized surface of the SS304 before the joining process. As the elemental distribution maps of Fe and Cr (Figs. 2b,c) show, the oxidized surface does not have a uniform distribution of these elements across its area. This can influence the nature of the phase(s) formed on the oxidized surface. So, for further examination, an elemental point analysis was performed on points A and B, which are illustrated in Fig. 2a. The results are presented in Table 3. Based on the relative count of the elements revealed at each point by the EDS detector and its comparison with the data in [28], the dominant phases of Cr_2O_3 and Fe_2O_3 were recognized for points A and B, respectively.

Although Cr_2O_3 is more stable than Fe_2O_3 at any temperature based on the principles of thermodynamics and only Cr_2O_3 was supposed to deposit on the oxidized surface, the results as to the presence of Fe_2O_3 in the oxidized surface imply a competition between thermodynamics and kinetics. This has been mentioned in [28, 29], in which it has been

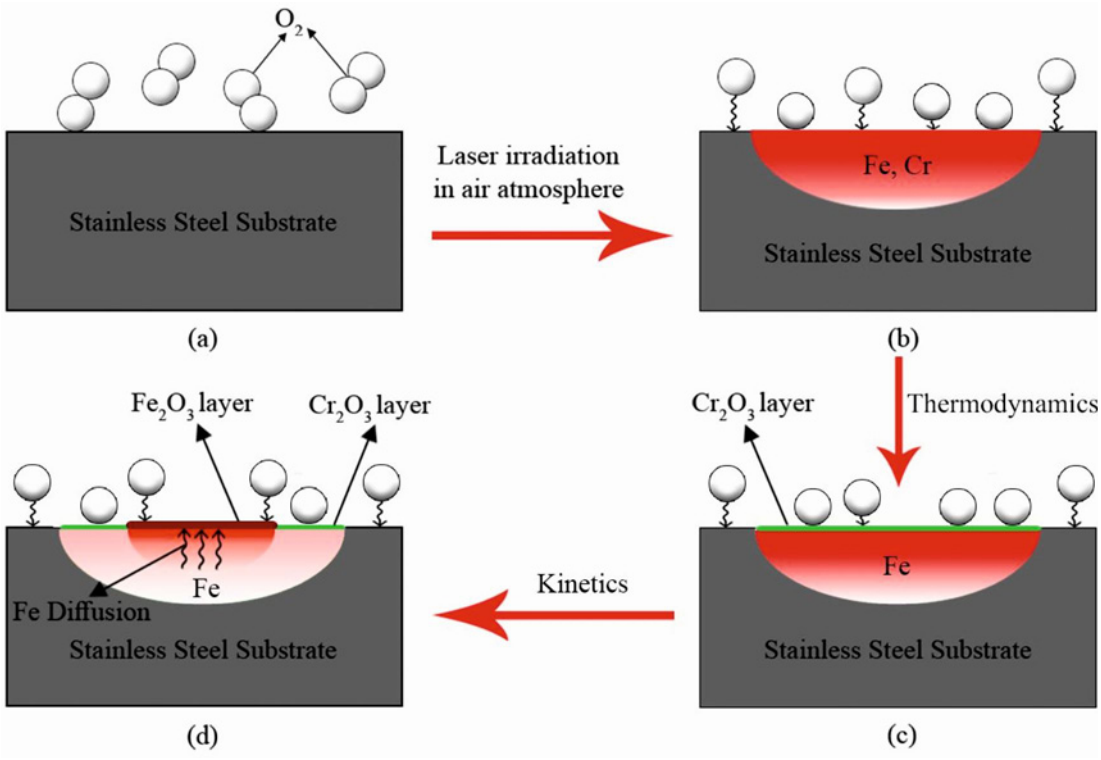

Fig. 3. A schematic of the oxidation mechanism of the stainless steel surface by laser scanning in the air atmosphere.

scrutinized. According to Fig. 3, the trend of surface oxidation of the SS304 can be better understood by laser scanning in the air atmosphere. So, when the stainless steel surface is radiated with the laser beam, oxygen molecules around the interaction zone are ionized (Figs. 3a,b). After the underlying layers absorb the oxygen ions/atoms, Cr preferentially reacts with oxygen, and a layer of Cr_2O_3 forms on the surface (Fig. 3c). Nevertheless, since Fe has a higher diffusion coefficient and the temperature is high enough at the center of the laser spot, Fe diffuses through Cr_2O_3. After it reacts with oxygen, a layer of Fe_2O_3 forms on the Cr_2O_3 surface layer (Fig. 3d). Consequently, two overlapped oxide films (Fe_2O_3 on Cr_2O_3) can be assumed in the central part. In addition, since Fe diffuses through the Cr_2O_3 layer, this layer may turn into a complex oxide film of Cr-Fe-O. However, at the edge of the laser spot, since the temperature is not high enough, Fe cannot diffuse through Cr_2O_3, and only Cr_2O_3 is observed. Given the lower density and adherence of Fe_2O_3 than Cr_2O_3 [30], this can affect joint strength adversely. However, based on the results of roughness measurement of the oxidized and non-oxidized metal surface just below the laser scanning path during joining (Table 4), it can be said that the metal oxidation process will be likely to improve joint strength due to the increased roughness of the metal surface at the joint zone and the resulting reinforcement of the mechanical interlocks at the joint interface.

Table 4. Mean roughness of oxidized and non-oxidized metal surfaces at the joint zone

Metal surface condition at the joint zone	Roughness (μm)
Non-oxidized	0.388
Oxidized	1.185

Figure 4 depicts SEM macrographs and the results of the related EDS line analysis (along the paths specified on each macrograph) from the cross-section of the pre-oxidized and non-pre-oxidized joints. The macrographs (Figs. 4a,b) show no apparent defects, such as numerous relatively large porosities induced by excessive thermal degradation of the polymer along the interface of both joints reported in [31]. In addition, although the results of the elemental linear analysis of the cross-section of both joints indicate that the width of the interaction zone (w) is almost equal for both joints, it can be observed that the weight percentage of oxygen in this zone is higher for the pre-oxidized joint (compare Figs. 4c,d). This can be attributed to the feasibility of increasing the formation of metal-oxygen-polymer bonds, reported in [15, 19, 20], the increased oxygen concentration in this zone of the pre-oxidized joint can remarkably influence the improvement of joint strength.

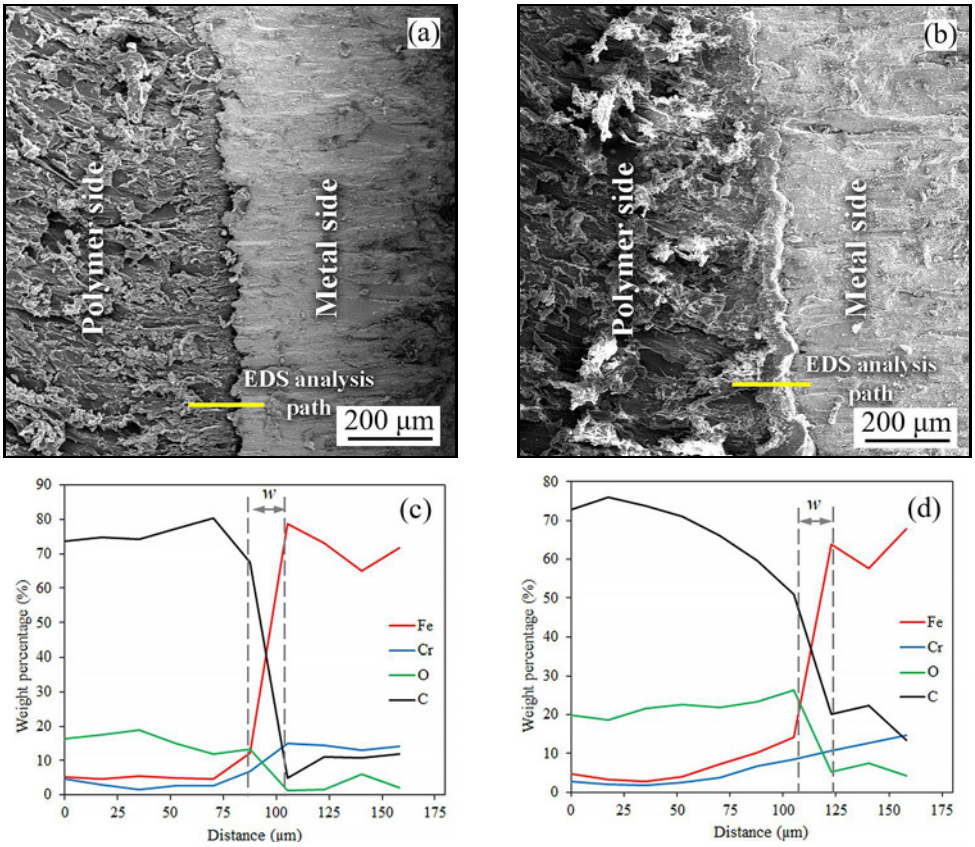

Fig. 4. SEM macrographs and the related EDS line analysis results along the paths specified on each macrograph from the cross-section of the pre-oxidized and non-pre-oxidized joints. (a), (c) are related to the non-pre-oxidized joint and (b), (d) are related to the pre-oxidized joint.

Table 5. Mean angular distortion of the joints

The surface condition of the metal component	Angular distortion, $\alpha(^\circ)$
Non-pre-oxidized	1.25 ± 0.07
Pre-oxidized	0.712 ± 0.08

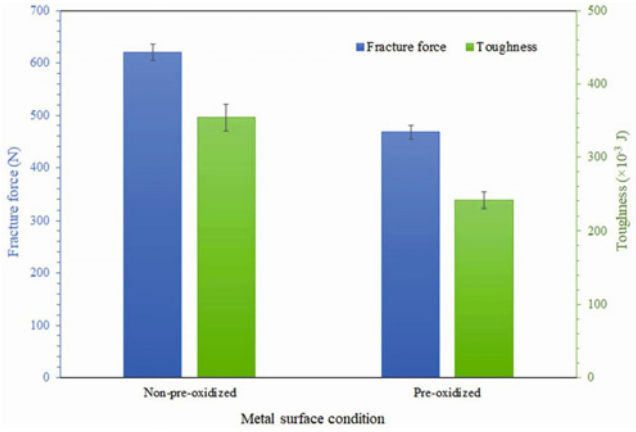

Fig. 5. Fracture force and toughness of the joints with different surface conditions of the metal component.

Before the tensile-shear test, the angular distortions of the pre-oxidized joint and the joint without surface pre-oxidation were compared to better understand their mechanical behavior. The results are provided in Table 5. As expected, the pre-oxidized joint had lower angular distortion because the distortion induced by the surface pre-oxidation treatment was in the opposite direction to the thermal stresses and the distortion induced by the joining process, so they partially neutralized one another. This can reduce the multidimensional stresses in the pre-oxidized joining zone during the tensile-shear test vis-à-vis the non-pre-oxidized joint.

Prior evidence suggests an improved joint due to strengthening metal-oxygen-polymer bonds by increasing the oxygen concentration at the joint zone, strengthening the mechanical interlocks at the interface, and even reducing the angular distortion through the metal surface oxidation pre-treatment. However, the results presented in Fig. 5 revealed that the fracture force of the pre-oxidized joint was significantly

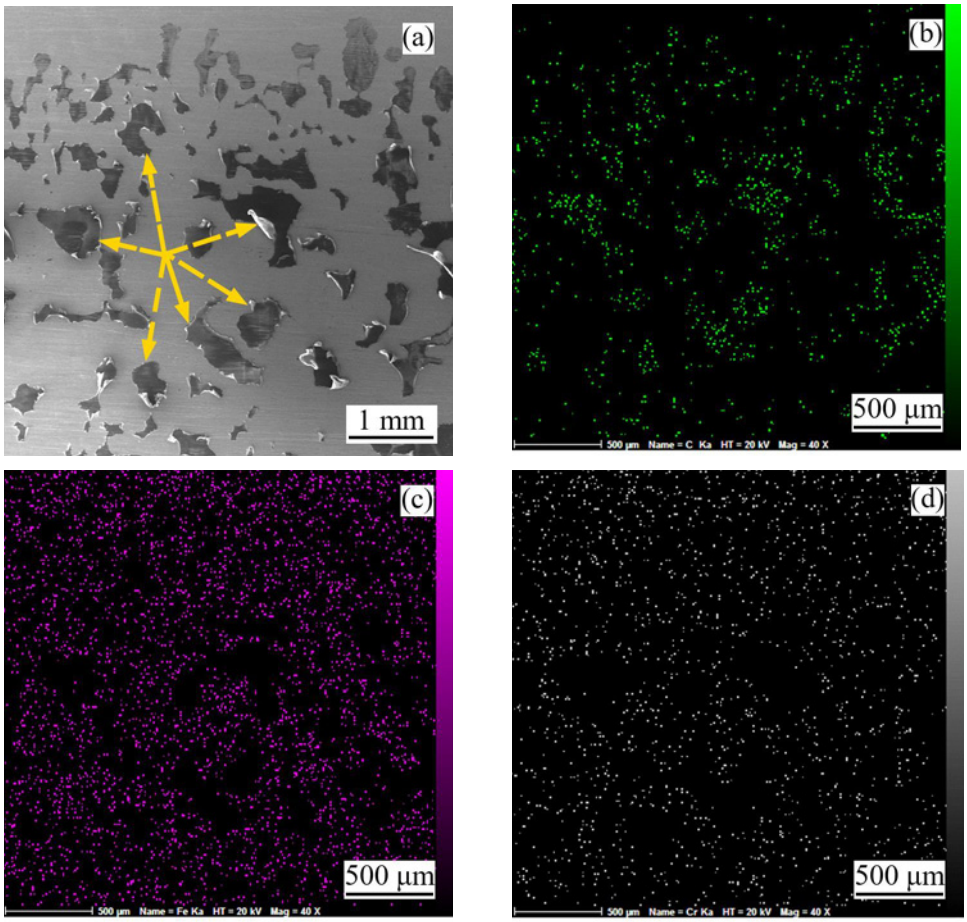

Fig. 6. (a) The morphology and elemental distribution maps of (b) C, (c) Fe, and (d) Cr on the metal-side fracture surface in the non-pre-oxidized joint. The dashed arrows in (a) show the residual polymers.

lower than that of the non-pre-oxidized joint. Two reasons can explain this difference in fracture force and the joints' toughness. First, when the surface pre-oxidation treatment is performed on the metal component, since the oxygen concentration at the surface layers of the metal increases, and the oxide film of the metal surface is reinforced at the joint zone, the heat conduction of the metal is disrupted at this zone so that it is reduced. Thus, less heat is transferred by the metal to the polymer during the joining process. This will reduce the wettability of the metal surface by the molten polymer, and since the effective joint area is reduced, the fracture force and toughness of the joint will decline versus the non-pre-oxidized state. The second reason is related to the nature of the oxide film formed on the stainless steel after the surface oxidation pre-treatment. As was already mentioned, Fe_2O_3 forms on a considerable area of the oxide film on the metal component for kinetic reasons, and since Fe_2O_3 has lower density and adherence than Cr_2O_3, it can impair the strength and toughness of the joint.

Nonetheless, to further explore the causes of the decline in the strength of the pre-oxidized joint and the impact of the above reasons, the joint zone was subjected to the fracture surfaces investigation, hardness test, and polymer differential scanning calorimetry analysis. The results are discussed below.

In the tensile-shear test, all joints were fractured by separation from the bond zone and some inside the polymer. Figures 6 and 7 display the morphology and elemental distribution maps of C, Fe, and Cr for the metal-side fracture surface in the non-pre-oxidized and pre-oxidized joints.

First, it is drawn from the comparison of the morphology and C distribution map on the metal-side fracture surface of the two joints (Figs. 6a,b and 7a,b) that the distribution of the residual polymer on the metal-side fracture surface was non-uniform in the pre-oxidized joint so that almost on the laser scanning path for the oxidation pre-treatment, a minimal amount of residual polymer was observed. This may support the reasons already mentioned for the decline in the mechanical properties of the pre-oxidized joint, i.e., lower wettability of the metal (due to the decrease in heat transfer by the metal at the oxidized zone) and weaker adherence of the oxide film (due to the presence of Fe_2O_3).

Second, the comparison of the Fe and Cr distri-

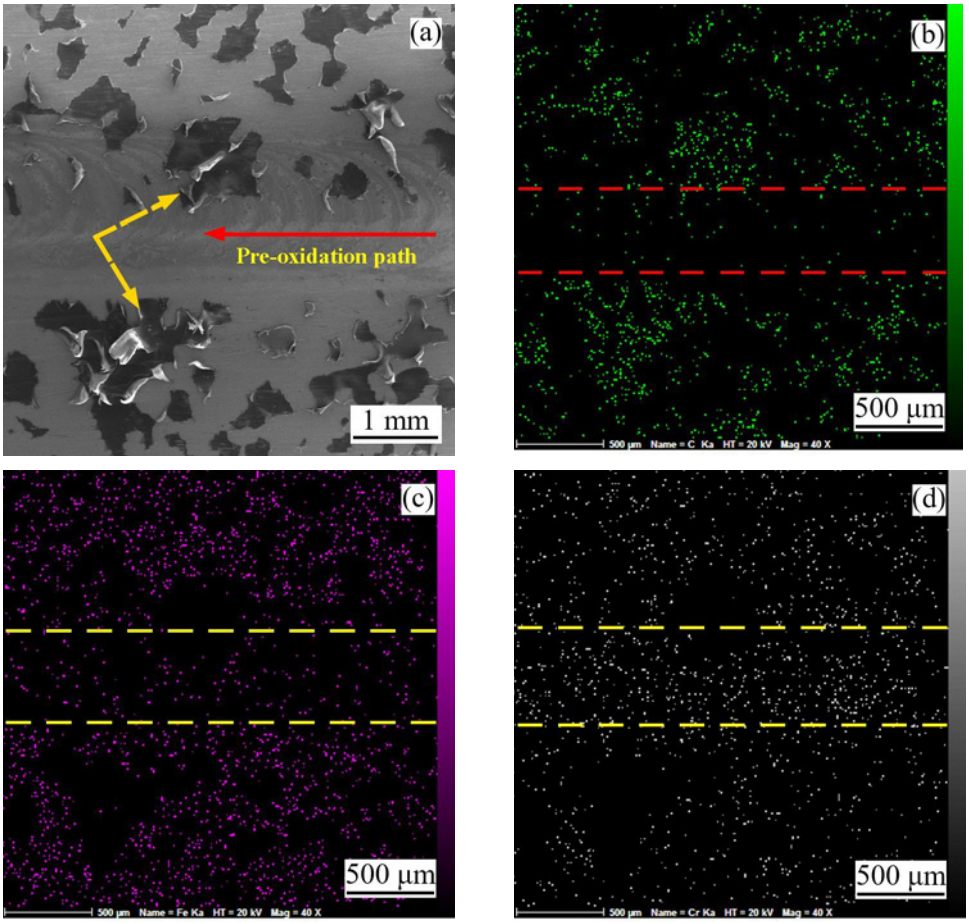

Fig. 7. (a) The morphology and elemental distribution maps of (b) C, (c) Fe, and (d) Cr of the metal-side fracture surface for the pre-oxidized joint. The dashed arrows in (a) and the distance between dashed lines in (b–d) show the residual polymers and the laser scanning path for the oxidation pre-treatment, respectively.

bution maps on the metal-side fracture surface in the two joints (Figs. 6c,d and Figs. 7c,d) reveals the non-uniform distribution of these elements on the pre-oxidized joint fracture surface so that almost on the right of the laser scanning path for the metal surface oxidation pre-treatment, less Fe but more Cr was present. However, as was already discussed in Fig. 3, the presence of these two elements on the path was expected to be the opposite. This may show the weak adherence of the oxide film (due to the presence of Fe_2O_3) on the metal surface of the pre-oxidized joint and, consequently, the reduction of the mechanical properties of this joint.

Figure 8 shows Fe morphology and elemental distribution map for the polymer-side fracture surface in the non-pre-oxidized and pre-oxidized joints. It is evident in Fig. 8a that the occasionally large porosities on the polymer-side fracture surface in the non-pre-oxidized joint show more thermal degradation of the polymer in the central zone of this joint. However, it is observed in the polymer-side fracture surface of the other joint (Fig. 8c) that the heat received during the joining process by the polymer in the zone of contact with the pre-oxidized metal surface was so slight that it inhibited the appropriate effect of heat on the polymer and this reduced the wettability of the metal surface. Indeed, this is associated with the reduction of heat transfer by the metal in the pre-oxidized zone, which impairs the mechanical properties of this joint. On the other hand, the concentrated and improper presence of Fe on the polymer-side fracture surface in the pre-oxidized joint (Fig. 8d) is good evidence of the second reason for the decline in the mechanical properties of the joint due to poor adherence of the iron oxide film formed on the metal surface after the oxidation pre-treatment.

Figure 9 depicts the base polymer differential scanning calorimetry analysis. Accordingly, the crystallinity percentage of the PA6 used in the joint was about 30 %, which was considered a criterion to compare the analysis results of polymer samples from the joint zone.

Table 6 presents the results of calculating the crystallinity percentage via differential scanning calorimetry and hardness measurement for the base polymer and the polymer of the joint zone in the pre-oxidized

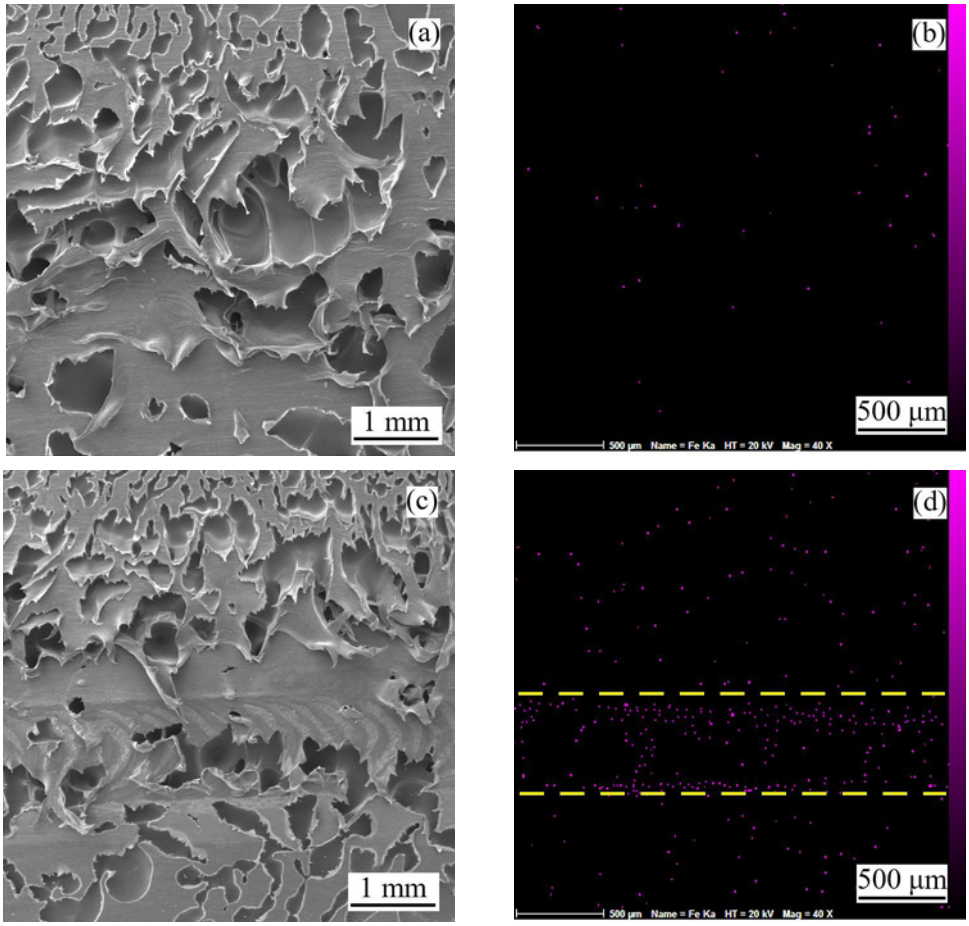

Fig. 8. The morphology and elemental distribution map of Fe on the polymer-side fracture surface in (a, b) non-pre-oxidized and (c, d) pre-oxidized joints. The area between dashed lines in (d) shows the region of the polymer surface that was in contact with the pre-oxidized zone on the metal surface.

Table 6. The crystallinity percentage and hardness of the base polymer and the polymer in the joint zone

Analysis location		Crystallinity percentage (%)	Hardness (Shore D)
Base polymer		30	61 ± 0.6
Polymer of the joint zone	Non-pre-oxidized joint	20.6	55 ± 0.8
	Pre-oxidized joint	24.4	57 ± 0.6

and non-pre-oxidized joints. The pre-oxidized joint recorded a closer hardness and crystallinity percentage to the base polymer than the non-pre-oxidized joint. This can be related to the exposure of the polymer to lower temperature variations (and consequently, the less reduction of its molecular weight) during the joining process due to the lower heat transfer by the metal in the pre-oxidized zone. This means less metal wettability by the polymer during joining in the pre-oxidized joint, which has led to a reduction in the effective area of the joint and a decrease in its strength. In other words, the difference between the two joints in the hardness and crystallinity percentage of the polymer in the joint zone demonstrates the reduction of metal wettability as the main cause of the decline in the mechanical properties of the pre-oxidized joint versus the non-pre-oxidized joint.

4. Conclusions

The present research explored the effect of laser pre-oxidation of stainless steel 304 for joining polyamide 6 by the LAMP method. Investigations were

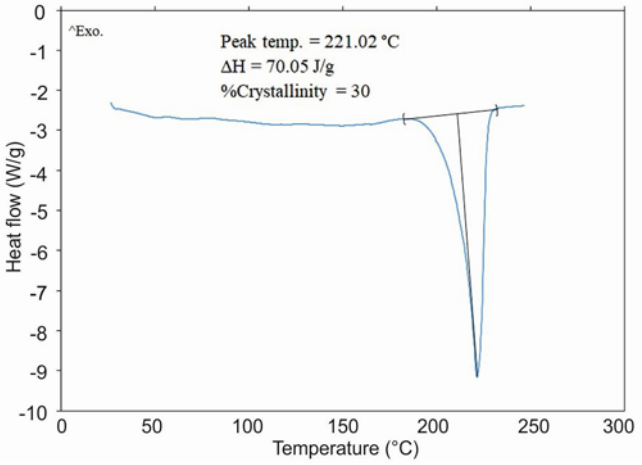

Fig. 9. The base polymer differential scanning calorimetry analysis.

made by the tensile-shear test, hardness measurement, roughness measurement, differential scanning calorimetry, and imagery and elemental analysis of the cross-sections and fracture surfaces of the joints. The most important results are briefly provided below:

1. The oxidation pre-treatment increases the surface roughness of the metal component and the oxygen concentration at the interface of the joint, which can potentially improve the strength of the joint by reinforcing mechanical interlocks and metal-oxygen-polymer bonds at the joint interface. Also, the reduction of angular distortion in the pre-oxidized joint due to the neutralization of heat stress and distortion induced by the oxidation pre-treatment and joining process can positively influence the mechanical behavior of the joint during loading.

2. However, the lower wettability of the metal by the polymer due to the reduction of heat transfer by the metal at the oxidized zone on the one hand and the weaker adherence of the oxide film formed on the surface of the stainless steel 304 due to the kinetic presence of Fe_2O_3 on the other have reduced the fracture force and toughness of the pre-oxidized joint (468 N, 241 mJ) by nearly 25 % as compared to the joint made with similar laser input energy but using non-pre-oxidized metal (620 N, 355 mJ).

3. It seems that to further improve metal-polymer joints, in addition to reinforcing the joining mechanisms by metal surface oxidation before the joining process, it is necessary to consider the nature of the oxide layer on the surface of the metal component of the joint and employ updated optimal variables of the joining process for the new surface conditions.

References

[1] J. Immarigeon, R. Holt, A. Koul, L. Zhao, W. Wallace, J. Beddoes, Lightweight materials for aircraft applications, Mater. Charact. 35 (1995) 41–67. https://doi.org/10.1016/1044-5803(95)00066-6

[2] W. Zhang, J. Xu, Advanced lightweight materials for automobiles: A review, Mater. Des. 221 (2022) 110994. https://doi.org/10.1016/j.matdes.2022.110994

[3] C. Magnus, Feasibility study of metal to polymer hybrid joining. [Ph.D. Thesis], Laboratory of Welding Technology of Department of Mechanical Engineering at Lappeenranta of Technology, Finland, 2012.

[4] F. Balle, G. Wagner, D. Eifler, Ultrasonic spot welding of aluminum sheet/carbon fiber reinforced polymer–joints, Materwiss. Werksttech. 38 (2007) 934–938. https://doi.org/10.1002/mawe.200700212

[5] N. Konchakova, F. Balle, F. Barth, R. Mueller, D. Eifler, P. Steinmann, Finite element analysis of an inelastic interface in ultrasonic welded metal/fibre-reinforced polymer joints, Comput. Mater. Sci. 50 (2010) 184–190. https://doi.org/10.1016/j.commatsci.2010.07.024

[6] S. Amancio-Filho, C. Bueno, J. Dos Santos, N. Huber, E. Hage Jr., On the feasibility of friction spot joining in magnesium/fiber-reinforced polymer composite hybrid structures, Mater. Sci. Eng. A 528 (2011) 3841–3848. https://doi.org/10.1016/j.msea.2011.01.085

[7] S. Goushegir, J. Dos Santos, S. Amancio-Filho, Friction spot joining of aluminum AA2024/carbon-fiber reinforced poly (phenylene sulfide) composite single lap joints: Microstructure and mechanical performance, Mater. Des. 54 (2014) 196–206. https://doi.org/10.1016/j.matdes.2013.08.034

[8] F. Khodabakhshi, M. Haghshenas, S. Sahraeinejad, J. Chen, B. Shalchi, J. Li, A. Gerlich, Microstructure-property characterization of a friction-stir welded joint between AA5059 aluminum alloy and high density polyethylene, Mater. Charact. 98 (2014) 73–82. https://doi.org/10.1016/j.matchar.2014.10.013

[9] F. Liu, J. Liao, K. Nakata, Joining of metal to plastic using friction lap welding, Mater. Des. 54 (2014) 236–244. https://doi.org/10.1016/j.matdes.2013.08.056

[10] S. Katayama, Y. Kawahito, Laser direct joining of metal and plastic, Scr. Mat. 59 (2008) 1247–1250. https://doi.org/10.1016/j.scriptamat.2008.08.026

[11] J. Holtkamp, A. Roesner, A. Gillner, Advances in hybrid laser joining, Int. J. Adv. Manuf. Technol. 47 (2010) 923–930. https://doi.org/10.1007/s00170-009-2124-6

[12] P. Woizeschke, V. Wottschel, Recent developments for laser beam joining of CFRP-Aluminum structures, Procedia Mat. Sci. 2 (2013) 250–258. https://doi.org/10.1016/j.mspro.2013.02.031

[13] M. Stambke, K. Schricker, J. P. Bergmann, A. Weiß, Laser-based joining of metal-thermoplastic tailored welded blanks, Weld. World 61 (2017) 563–573. https://doi.org/10.1007/s40194-017-0429-x

[14] C. Ageorges, L. Ye, Resistance welding of metal/thermoplastic composite joints, J. Thermoplast. Compos. Mater. 14 (2001) 449–475. https://doi.org/10.1106/PN74-QXKH-7XBE-XKF5

[15] K. Jung, Y. Kawahito, S. Katayama, Laser direct joining of carbon fibre reinforced plastic to stainless steel, Sci. Technol. Weld. Join. 16 (2011) 676–680. https://doi.org/10.1179/1362171811Y.0000000060

[16] J. Jiao, Z. Xu, Q. Wang, L. Sheng, W. Zhang, CFRTP and stainless steel laser joining: Thermal defects analysis and joining parameters optimization, Opt. Laser

Technol. 103 (2018) 170–176.
https://doi.org/10.1016/j.optlastec.2018.01.023
[17] K. Schricker, L. Samfaß, M. Grätzel, G. Ecke, J. P. Bergmann, Bonding mechanisms in laser-assisted joining of metal-polymer composites, J. Adv. Join. Process. 1 (2020) 100008.
https://doi.org/10.1016/j.jajp.2020.100008
[18] S. Arai, Y. Kawahito, S. Katayama, Effect of surface modification on laser direct joining of cyclic olefin polymer and stainless steel, Mater. Des. 59 (2014) 448–453.
https://doi.org/10.1016/j.matdes.2014.03.018
[19] D.-J. Jung, J. Cheon, S.-J. Na, Effect of surface pre-oxidation on laser assisted joining of acrylonitrile butadiene styrene (ABS) and zinc-coated steel, Mater. Des. 99 (2016) 1–9.
https://doi.org/10.1016/j.matdes.2016.03.044
[20] Z. Zhang, J.-G. Shan, X.-H. Tan, J. Zhang, Effect of anodizing pre-treatment on laser joining CFRP to aluminum alloy A6061, Int. J. Adhes. Adhes. 70 (2016) 142–151.
https://doi.org/10.1016/j.ijadhadh.2016.06.007
[21] E. Rodríguez-Vidal, C. Sanz, C. Soriano, J. Leunda, G. Verhaeghe, Effect of metal micro-structuring on the mechanical behavior of polymer-metal laser T-joints, J. Mater. Process. Technol. 229 (2016) 668–677.
https://doi.org/10.1016/j.jmatprotec.2015.10.026
[22] L. Sheng, C. Lai, Z. Xu, J. Jiao, Effect of the surface texture on laser joining of a carbon fiber-reinforced thermosetting plastic and stainless steel, Strength Mater. 51 (2019) 122–129.
https://doi.org/10.1007/s11223-019-00057-w
[23] J. Jiao, S. Jia, Z. Xu, Y. Ye, L. Sheng, W. Zhang, Laser direct joining of CFRTP and aluminium alloy with a hybrid surface pre-treating method, Compos. B Eng. 173 (2019) 106911.
https://doi.org/10.1016/j.compositesb.2019.106911
[24] Y. Ye, Q. Zou, Y. Xiao, J. Jiao, B. Du, Y. Liu, L. Sheng, Effect of interface pretreatment of Al alloy on bonding strength of the laser joined Al/CFRTP butt joint, Micromachines 12 (2021) 179.
https://doi.org/10.3390/mi12020179
[25] R. Ghanavati, E. Ranjbarnodeh, R. Shoja-Razavi, G. Pircheraghi, Experimental and numerical investigation of the effect of laser input energy on the mechanical behavior of stainless steel and polyamide joint in the LAMP joining method, Int. J. Adv. Manuf. Technol. 113 (2021) 3585–3597.
https://doi.org/10.1007/s00170-021-06859-0
[26] A. Al-Sayyad, P. Lama, J. Bardon, P. Hirchenhahn, L. Houssiau, P. Plapper, Laser joining of titanium alloy to polyamide: Influence of process parameters on the joint strength and quality, Int. J. Adv. Manuf. Technol. 107 (2020) 2917–2925.
https://doi.org/10.1007/s00170-020-05123-1
[27] W. Sichina, DSC as problem solving tool: Measurement of percent crystallinity of thermoplastics, Perkin Elmer Instruments and PETech. 40 (2000).
[28] C. Cui, X. Cui, X. Ren, M. Qi, J. Hu, Y. Wang, Surface oxidation phenomenon and mechanism of AISI 304 stainless steel induced by Nd: YAG pulsed laser, Appl. Surf. Sci. 305 (2014) 817–824.
https://doi.org/10.1016/j.apsusc.2014.04.025
[29] D. P. Adams, V. Hodges, D. Hirschfeld, M. A. Rodriguez, J. McDonald, P. G. Kotula, Nanosecond pulsed laser irradiation of stainless steel 304L: Oxide growth and effects on underlying metal, Surf. Coat. Technol. 222 (2014) 1–8.
https://doi.org/10.1016/j.surfcoat.2012.12.044
[30] H. Rojacz, F. Birkelbach, L. Widder, M. Varga, Scale adhesion, scratch and fracture behaviour of different oxides formed on iron based alloys at 700 °C, Wear 380 (2017) 126–136.
https://doi.org/10.1016/j.wear.2017.01.004
[31] J. Jiao, Q. Wang, F. Wang, S. Zan, W. Zhang, Numerical and experimental investigation on joining CFRTP and stainless steel using fiber lasers, J. Mater. Process. Technol. 240 (2017) 362–369.
https://doi.org/10.1016/j.jmatprotec.2016.10.013